Modes of eastern equatorial Pacific thermocline variability: Implications for ENSO dynamics over the last glacial period

Guillaume Leduc,[1,2] Laurence Vidal,[1] Olivier Cartapanis,[1] and Edouard Bard[1]

Received 15 October 2008; revised 11 May 2009; accepted 4 June 2009; published 23 July 2009.

[1] Changes in El Niño–Southern Oscillation (ENSO) variability are difficult to extract from paleoceanographic reconstructions because they are superimposed on changes in seasonal variability that modulate the first-order climate signal. Here we address this problem by reconstructing thermocline structure from a marine sediment core retrieved from the eastern equatorial Pacific. At the core location, changes in hydrologic parameters within the thermocline are linked to ENSO activity, with a reduced influence of seasonal variability compared to surface waters. We performed repeated isotopic analyses ($\delta^{18}O$) on single specimens of the thermocline-dwelling planktonic foraminifera *Neogloboquadrina dutertrei* at several targeted time periods over the last 50 ka to extract the total thermocline variance, a parameter supposed to reveal changes in ENSO. No fundamental changes in amplitude and frequency of the events were detected despite differences in climatic background. However, our data suggest that long-term variations in the thermocline variability occurred over the last 50 ka, with the highest and lowest ENSO activities occurring during the last glacial period and the Last Glacial Maximum, respectively.

Citation: Leduc, G., L. Vidal, O. Cartapanis, and E. Bard (2009), Modes of eastern equatorial Pacific thermocline variability: Implications for ENSO dynamics over the last glacial period, *Paleoceanography*, *24*, PA3202, doi:10.1029/2008PA001701.

1. Introduction

[2] El Niño–Southern Oscillation (ENSO) is an interannual climatic phenomenon originating in the tropical Pacific Ocean and is due to disturbances in the Walker atmospheric circulation [*Rasmusson and Carpenter*, 1982]. At the onset of El Niño events, trade winds weaken and induce the eastward migration of deep atmospheric convection sites normally localized above the Western tropical Pacific warm pool. In the eastern equatorial Pacific (EEP) the thermocline deepens and Sea Surface Temperatures (SST) show positive anomalies of several degrees [*Rasmusson and Carpenter*, 1982]. ENSO has worldwide repercussions through ocean-atmosphere interactions and climatic teleconnections [*Cane*, 1998; *Liu and Alexander*, 2007; *Emile-Geay et al.*, 2007].

[3] Paleoreconstructions [*McCulloch et al.*, 1996; *Corrège et al.*, 2000; *Tudhope et al.*, 2001; *Koutavas et al.*, 2002; *Moy et al.*, 2002; *Stott et al.*, 2002; *Koutavas and Lynch-Stieglitz*, 2003; *Cobb et al.*, 2003; *Martínez et al.*, 2003; *Turney et al.*, 2004; *Cane*, 2005; *Rein et al.*, 2005; *Koutavas et al.*, 2006; *Conroy et al.*, 2008; *Pena et al.*, 2008; *Grelaud et al.*, 2009] and modeling experiments [*Clement et al.*, 1999, 2001; *Otto-Bliesner et al.*, 2003; *Timmermann et al.*, 2005; *Otto-Bliesner et al.*, 2006; *Timmermann et al.*, 2007; *Brown et al.*, 2008; *Zheng et al.*, 2008] attempting to reconstruct past changes in ENSO have indicated a wide range of potential mechanisms hypothesized to have influenced the ENSO variability. However, most of these mechanisms and their impacts on ENSO remain controversial (see, e.g., *Corrège et al.* [2000] versus *Moy et al.* [2002] for the mid-Holocene, *Koutavas et al.* [2002] versus *Martínez et al.* [2003] for the Last Glacial Maximum (LGM), *Stott et al.* [2002] versus *Turney et al.* [2004] for the Heinrich/Dansgaard-Oeschger (H/DO) millennial-scale climate variability, etc.)

[4] One cause for conflicting results is that extracting an unequivocal ENSO variability spectrum in ENSO-sensitive regions remains difficult since changes in seasonal variability generate first-order climatic signals [*Denton et al.*, 2005; *Braconnot et al.*, 2007b; *Flückiger et al.*, 2008; *Timm et al.*, 2008]. To date, fossil corals remain the best archive for reconstructing past ENSO variability since they contain both seasonal and interannual variability [*Fairbanks et al.*, 1997; *Tudhope et al.*, 2001; *Cobb et al.*, 2003]. The drawback is that they are restricted in time to several centuries. Theoretically, marine sediment archives can provide valuable information on ENSO variability in the past. However, efforts to identify and separate the effects of seasonal variability from ENSO are necessary.

[5] In this study, we explored a way of reducing seasonal overprints inherent in paleo-ENSO reconstructions by extracting the EEP thermocline variability spectrum in a marine sediment core. At core site, thermocline variability is significantly influenced by ENSO (Figures 1 and 2), but with a secondary role of seasonal variability compared with surface hydrologic conditions (Figure 2). The planktonic foraminifera *Neogloboquadrina dutertrei* lives in the thermocline, making it a suitable species to detect past changes in the thermocline structure due to ENSO. We performed repeated isotopic analysis ($\delta^{18}O$) on single specimen of *N. dutertrei* to extract snapshots of the thermocline variability spectrum, a parameter assumed to reveal changes in ENSO. The variances of individual *N. dutertrei* $\delta^{18}O$ measurements

[1] CEREGE, Aix-Marseille Université, Collège de France, IRD, CNRS, Aix-en-Provence, France.
[2] Now at Institut für Geowissenschaften, Christian Albrecht Universität, Kiel, Germany.

0883-8305/09/2008PA001701$12.00

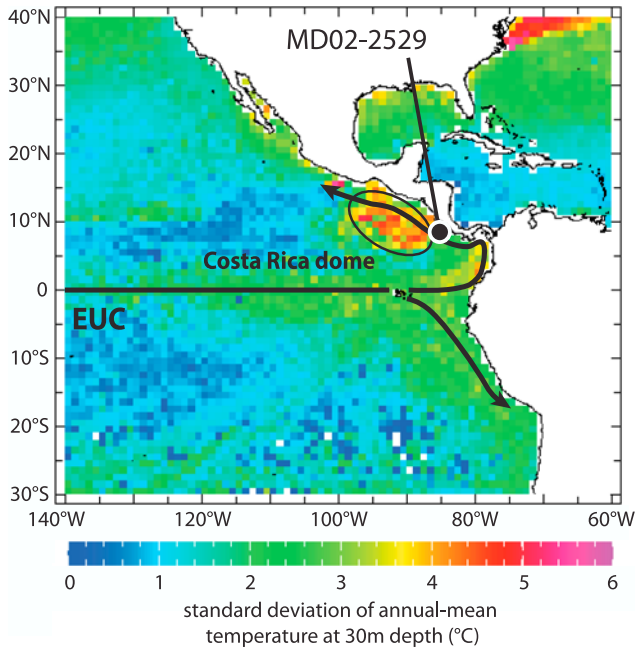

Figure 1. Map of the standard deviation for the annual mean temperature at 30 m depth (i.e., a record of interannual temperature variability at this depth). Data are from the WOA01 database [*Conkright et al.*, 2002]. Also shown is the MD02-2529 core location, the mean Costa Rica Dome location [*Fiedler*, 2002], and the main undercurrent paths derived from the Equatorial Undercurrent (EUC).

give new insights regarding past changes in the mean state of ENSO activity (i.e., a mixture of both the amplitude and frequency of ENSO events).

2. Oceanographic Background

2.1. EEP Hydrology

[6] Surface hydrologic variability at the MD02-2529 core location is primarily influenced by seasonal variations in precipitation rates and wind-driven surface currents that are set up by latitudinal movements of the Intertropical Convergence Zone (ITCZ), while ENSO exerts a limited effect on surface hydrologic parameters [*Linsley et al.*, 1994; *Leduc et al.*, 2007]. A sharp thermocline occurs between 30 and 70 m, with a temperature difference larger than 10°C (Figure 2a). The halocline separates surface waters with salinities lower than 33 psu from subsurface waters with salinities higher than 35 psu (Figure 2a). The combined temperature and salinity effects make the EEP the region with the strongest pycnocline in the world ocean, thus providing efficient stratification between surface and subsurface waters [*Fiedler and Talley*, 2006]. At the site studied, the pycnocline has remained stable for the last 90 ka, despite abrupt variations in the Central American monsoon that affected surface hydrologic changes (see supplementary information in the work by *Leduc et al.* [2007]).

[7] EEP subsurface waters are bathed by the eastern end path of the Equatorial Undercurrent (Figure 1), with full seasonal amplitudes in temperature and salinity variations up to ~4°C and ~2 psu, respectively (Figure 2a) [*Fiedler and Talley*, 2006]. The interannual temperature variability of the thermocline is larger than 4°C at the core location (Figure 1), with +2 to +3°C temperature anomalies averaged over El Niño years (−0.5 to −2°C over La Niña years) (Figure 2c), indicating that foraminifera living within the thermocline are impacted by ENSO variability. Thermocline variability is slightly amplified at the MD02-2529 core location because it is located at the edge of the Costa Rica Dome (CRD), known to expand and contract in size with ENSO activity (Figure 1) [*Fiedler*, 2002].

2.2. *N. dutertrei* as a Recorder of Thermocline Variability

[8] In the EEP region, a series of field studies have provided insight regarding the vertical distribution of planktonic foraminifera and their corresponding stable isotopic ratios [*Fairbanks et al.*, 1982] (Figure 2d), as well as the seasonal variability of planktonic foraminifera fluxes [*Thunell et al.*, 1983] and their stable isotopic signatures [*Curry et al.*, 1983]. The entire *N. dutertrei* inventory indicates a living depth range from the surface to waters deeper than 200 m, with an associated increase in $\delta^{18}O$ signatures. For this reason, a large scattering in individual *N. dutertrei* $\delta^{18}O$ signature is awaited because of habitat depth. However, maximum *N. dutertrei* abundance is found within the thermocline (Figure 2d; note the logarithmic scale [*Fairbanks et al.*, 1982]), i.e., where maximum interannual temperature anomalies are found (Figures 1 and 2c). This ecological preference is supported by Mg/Ca measurements performed on *N. dutertrei* from marine sediments retrieved in the Galapagos region, where core top temperatures are consistent with the present-day thermocline temperature [*Pena et al.*, 2008].

[9] The reason for *N. dutertrei* subsurface ecological preference is linked to the subsurface chlorophyll maximum [*Fairbanks et al.*, 1982], which is set up by the pycnocline where a close association between phytoplanktonic and zooplanktonic communities develops [*Fairbanks and Wiebe*, 1980]. Strong thermocline structure changes linked to ENSO variability do not alter the depth of the pycnocline since the halocline is poorly altered by ENSO variability [*Fiedler and Talley*, 2006], suggesting that the depth of the chlorophyll maximum and hence *N. dutertrei* habitat is not strongly altered by ENSO variability.

2.3. Link Between Hydrologic Conditions Recorded by *N. dutertrei* $\delta^{18}O$ and Thermocline Variability

[10] The $\delta^{18}O$ measured on foraminifera tests is a function of both temperature and the $\delta^{18}O$ of seawater ($\delta^{18}O_{sw}$), the latter being linearly related to salinity (see *Fairbanks et al.* [1982] and *Benway and Mix* [2004] for the regional salinity/$\delta^{18}O_{sw}$ relationship). In Figure 3a, the $\delta^{18}O_{sw}$ and water temperature evolution at a water depth of 50 m at the MD02-2529 core location are compared for the period from 1980 to 2000 A.D. in order to evaluate the effect of ENSO variability on subsurface hydrology. During the peak of El Niño warm events, the temperature effect (~8°C) on the $\delta^{18}O$ of calcium carbonate at equilibrium is larger in magnitude in a fourfold range than the $\delta^{18}O_{sw}$ (~0.25‰) (Figure 3a). Both parameters act together to enhance the

response of the expected $\delta^{18}O$ of the *N. dutertrei* signal, avoiding the need to disentangle the temperature and salinity effects on calcium carbonate $\delta^{18}O$ (Figure 3a). When the expected $\delta^{18}O$ of calcite at 50 m depth is computed for this time interval with the data set shown in Figure 3a, its temporal variability for the 1980–2000 A.D. period is significantly correlated to the Southern Oscillation Index (SOI), with a level of significance higher than 99% (r^2 = 0.27, n = 252) (Figure 3b). When the 3-month lag in thermocline variability with respect to the SOI is corrected, the correlation is even enhanced (r^2 = 0.35, n = 249). The lag reflects the "delayed oscillator" conceptual model that

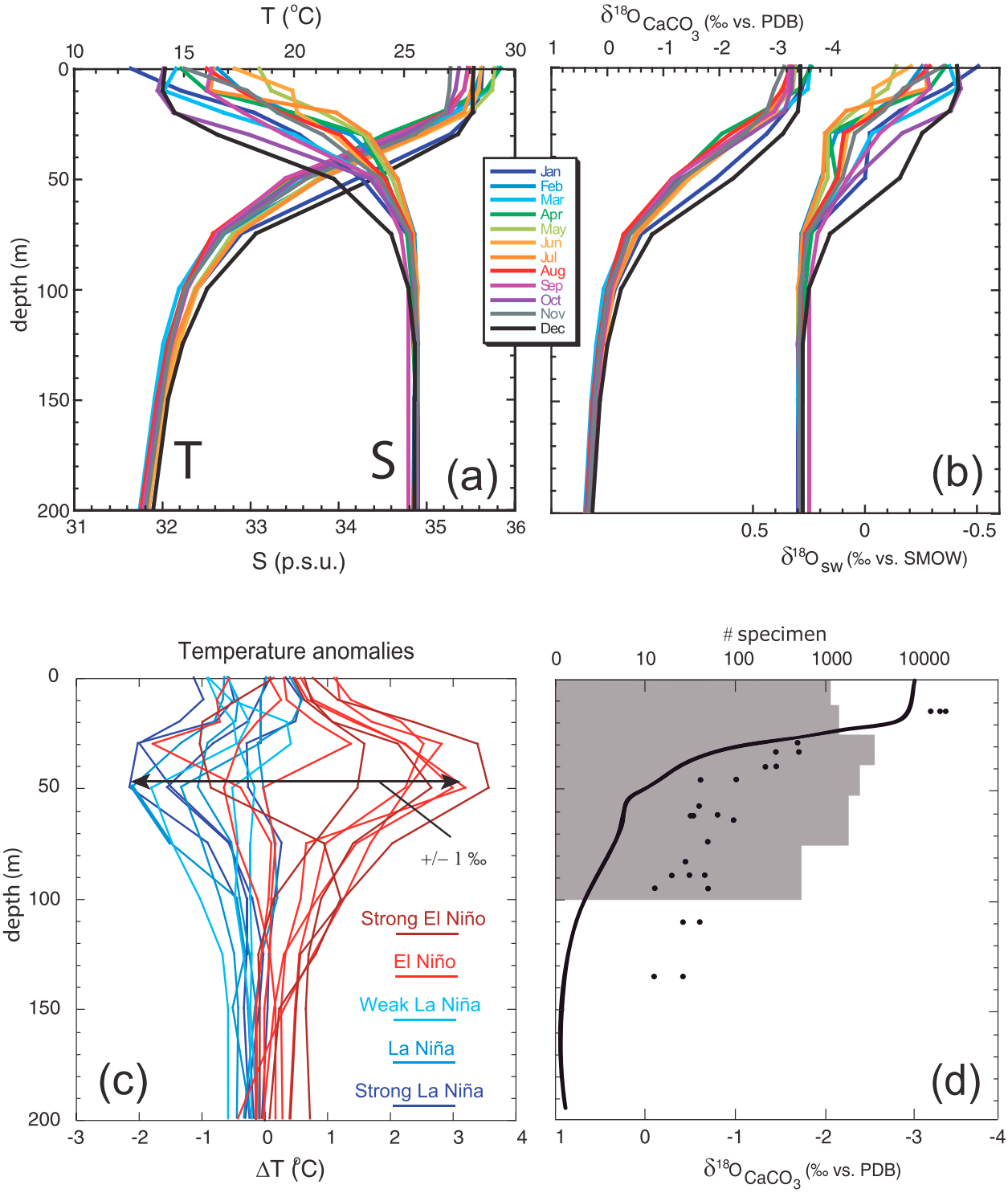

Figure 2

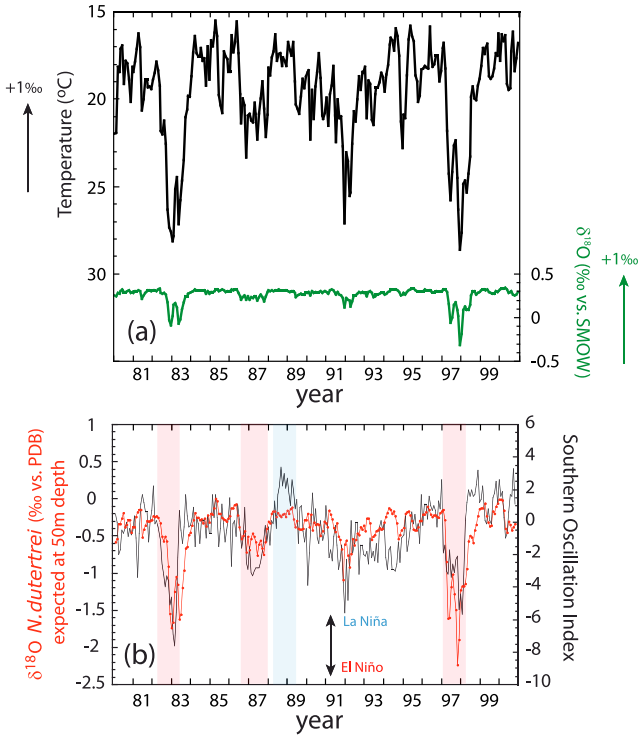

Figure 3. (a) Temporal variations of hydrologic parameters at 50 m water depth at the core location compared to (b) the Southern Oscillation Index (SOI) for the 1980–2000 A.D. period. Figure 3a shows temperature (black curve) and calculated $\delta^{18}O_{sw}$ values from salinities with the $\delta^{18}O_{sw}$/salinity relationship described in Figure 2 (green curve). The arrow gives an approximation of the temperature and the $\delta^{18}O_{sw}$ impact on $\delta^{18}O_{CaCO3}$. Figure 3b shows expected $\delta^{18}O_{CaCO3}$ at equilibrium calculated using the data set shown in Figure 3a (red curve) and compared to the SOI (black curve). Hydrologic data are from NCEP/NCAR reanalysis (http://iridl.ldeo.columbia.edu/). Major El Niño and La Niña events for this time period are indicated by red and blue, respectively.

explains the oscillatory nature of ENSO, and is illustrated by the thermocline response lag with respect to the atmospheric signal in Figure 3b (e.g., see the review of *Wang* [2001] for a detailed description of this process).

[11] *N. dutertrei* has already been successfully used to reconstruct past EEP upper water column thermal structure [*Patrick and Thunell*, 1997; *Faul et al.*, 2000; *Spero et al.*, 2003; *Pena et al.*, 2008]. In order to extract the entire hydrologic variability range for several targeted time slices, we performed repeated analyses of $\delta^{18}O$ on single planktonic foraminifera specimens, as it has been done by *Billups and Spero* [1996] and *Koutavas et al.* [2006]. Our expectation was that individual $\delta^{18}O$ measurements of *N. dutertrei* would provide an efficient strategy for extracting the full thermocline variability range, that ultimately represents a snapshot of ENSO activity for various time slices. Sedimentation rates ranging from 13 to more than 20 cm ka^{-1} in core MD02-2529 reduced the bioturbation effect [*Bard*, 2001].

3. Analytical Procedure

[12] The MD02-2529 sediment core (08°12.33′N, 84°07.32′W, 1619 m water depth) was collected using the Calypso corer aboard the French R.V. *Marion Dufresne* in June 2002 during the IMAGES VIII/MONA campaign (the campaign was dedicated to the study of the Northwestern America Margin). We performed repeated analyses on single specimens of *N. dutertrei* from the MD02-2529 core which has a well-established stratigraphy [*Leduc et al.*, 2007]. Approximately 80 single *N. dutertrei* specimens were analyzed for several targeted time slices spanning the last 50 ka (i.e., during the Holocene, the Last Glacial Maximum, Dansgaard-Oeschger interstadials 8 and 14, and Heinrich events 1 and 4). For stable isotopic measurements, *N. dutertrei* were selected from the > 250 μm size fraction with tests weights ranging from ~40 and 60 μg. Samples were subjected to a reaction with H_3PO_4 at 70°C and the evolved CO_2 was analyzed using a Finnigan Delta Advantage mass spectrometer at CEREGE. Stable isotopic ratios are reported in ‰ relative to the Vienna Peedee belemnite standard, with $\delta^{18}O = [(^{18}O/^{16}O_{sample}/^{18}O/^{16}O_{standard}) - 1]1000$. Analytical precision was better than ±0.05‰ (±1σ) for the $\delta^{18}O$ on the basis of repeated analyses of a National Bureau Standard (NBS-19) limestone standard.

[13] The MD02-2529 age model is based on radiocarbon measurements performed on planktonic foraminifera for the last 40 ka, and on benthic isotopic stratigraphy for the 40–70 ka B.P. time interval (see *Leduc et al.* [2007] for a more detailed description of the age model). In a previous

Figure 2. (a and b) Monthly hydrologic records of the upper 200 m depth at core location compared to (c) the annual temperature anomalies associated with ENSO dynamics at the MD02-2529 core location and (d) the ecological characteristics of *N. dutertrei*. Temperature and salinity were extracted from the WOA01 database [*Conkright et al.*, 2002] (Figure 2a). The values of $\delta^{18}O$ calculated for the seawater and for the $CaCO_3$ at equilibrium are based on the same data set (Figure 2b). To convert the salinity to $\delta^{18}O_{sw}$, we used the $\delta^{18}O_{sw}$-salinity relationship ($\delta^{18}O_{sw}$ (‰) = 0.253S (psu) − 8.52 for the upper 40 m water depth and $\delta^{18}O_{sw}$ (‰) = 0.471S (psu) − 16.15 for the 40–200 m water depth interval [*Benway and Mix*, 2004]). The $\delta^{18}O_{CaCO3}$ was calculated using the paleotemperature equation of *O'Neil et al.* [1969] (T (°C) = 16.9 − 4.38 ($\delta^{18}O_{CaCO3} - \delta^{18}O_{sw}$) + 0.1 ($\delta^{18}O_{CaCO3} - \delta^{18}O_{sw}$)^2). Figure 2c shows annual temperature anomalies for the years of El Niño or La Niña during the 1950–2004 period according to the census list of El Niño and La Niña years (http://ggweather.com/enso/years.htm). The arrow indicates by how much the $\delta^{18}O$ of calcite will be impacted by temperature anomalies at the depth of the thermocline. Figure 2d shows expected $\delta^{18}O_{CaCO3}$ at equilibrium (black curve) compared to the $\delta^{18}O$ measured for *N. dutertrei* (dots) and to vertical distribution of living *N. dutertrei* in the Panama Basin (in specimens per 1000 m^3 (gray shaded histograms); note the logarithmic scale) [*Fairbanks et al.*, 1982].

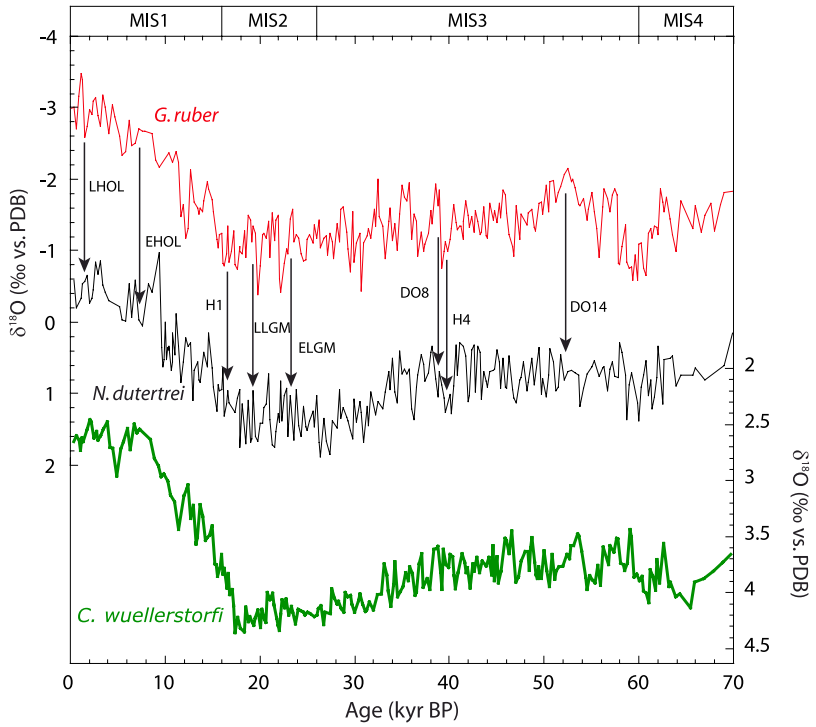

Figure 4. Temporal variations in $\delta^{18}O$ measurements performed on multiple specimens of *G. ruber* (red curve [*Leduc et al.*, 2007]), *N. dutertrei* (black curve, this study), and *C. wuellerstorfi* (green curve [*Leduc et al.*, 2007]) over the last 70 ka. Arrows localize the time slices chosen for repeated analyses of individual *N. dutertrei*. LHOL, late Holocene; EHOL, early Holocene; H1, Heinrich event 1; LLGM, late Last Glacial Maximum; ELGM, early Last Glacial Maximum; DO8, Dansgaard-Oeschger interstadial 8; H4, Heinrich event 4; and DO14, Dansgaard-Oeschger interstadial 14. Marine isotopic stages are labeled at top of the plot.

study it was demonstrated that the $\delta^{18}O$ of the surface-dwelling planktonic foraminifera species *Globigerinoides ruber* recorded changes in the hydrologic cycle, which were linked to changes in ITCZ dynamics and related moisture transport across Central America that acted to amplify the *G. ruber* isotopic response at the coring site [*Leduc et al.*, 2007]. Since these changes occurred in concert with Heinrich/Dansgaard-Oeschger events, the $\delta^{18}O$ of *G. ruber* was used as a stratigraphic tool for identifying times for rapid climate changes in the sedimentary sequence. Down-core measurements were performed over the last 70 ka at a centennial time resolution using 2 to 3 specimens (Figure 4). Then, several targeted time intervals were chosen for repeated analysis on *N. dutertrei* single specimen (Figure 4). Approximately 60 to 90 specimens were picked from a 1-cm-wide sediment sample, except for the Holocene and for the marine isotope stage (MIS) 2 time slices where there were not sufficient *N. dutertrei* found to produce data sets from a 1-cm-wide sediment sample (Table 1). For these time slices we performed measurements on wider sedimentary intervals,

Table 1. Sedimentary and Statistical Results for Each Time Slice[a]

	LHOL	EHOL	H1	LLGM	ELGM	DO8	H4	DO14
Approximate age (ka)	1.5	7	16.5	19.4	23.6	38.9	39.6	52.1
Sedimentation rate (cm ka^{-1})	44	29	17	15	15	16	16	13
Sample interval width (cm)	4	5	1	3	9	1	1	1
Integrated time (years)	91	172	59	200	600	62	62	77
Number of individual analysis	81	72	67	67	70	88	76	89
Total $\delta^{18}O$ range	1.75	1.72	1.52	1.62	1.60	1.99	2.10	1.94
Mean $\delta^{18}O$	−0.33	0.18	0.85	1.19	1.36	0.73	0.81	0.45
σ $\delta^{18}O$	0.38	0.36	0.34	0.32	0.35	0.41	0.42	0.47
σ_T $\delta^{18}O$ (Jackknife)	0.066	0.065	0.065	0.063	0.065	0.066	0.069	0.071

[a]See text for details on statistical methods. LHOL, late Holocene; EHOL, early Holocene; H1, Heinrich event 1; LLGM, late Last Glacial Maximum; ELGM, early Last Glacial Maximum; DO8, Dansgaard-Oeschger interstadial 8; H4, Heinrich event 4; and DO14, Dansgaard-Oeschger interstadial 14.

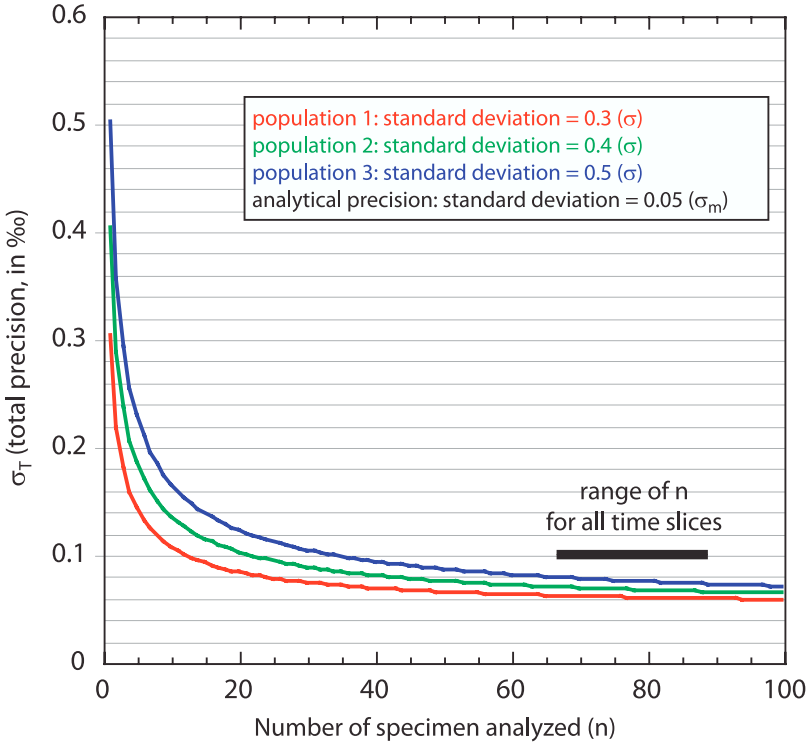

Figure 5. Estimation of total precision on the estimated variance of one population (here *N. dutertrei* δ^{18}O measurements for one time slice) as a function of the number of individual foraminifera specimens analyzed. The variances of one δ^{18}O population (here 0.3, 0.4, and 0.5 in red, green, and blue, respectively) and the variance of the analytical procedure (0.05) are given. The range of the population size for all time slices is indicated as a black bar.

ranging from 3 to 9 cm. A synthesis of the individual analyses is reported in Table 1.

[14] Since the number of individual *N. dutertrei* δ^{18}O samples analyzed varies among the time intervals studied, we utilize a Jackknife statistical technique to estimate the degree of precision attained using an estimation of δ^{18}O population variance [*Schiffelbein and Hills*, 1984]. Such an estimation is based on the following equation that measures the total precision of the calculated standard deviation (SD) in one population:

$$\sigma_T^2 = \sigma_m^2 + (\sigma^2/n)$$

where σ_T is the total δ^{18}O variance precision, σ_m is the analytical SD of δ^{18}O measurements given by the machine's precision (0.05 in our case), σ is the calculated SD for the δ^{18}O measurements, and n is the number of individuals analyzed. The σ_T was computed as a function of the number of foraminifera analyzed, assuming a SD with values of 0.3, 0.4, and 0.5, bracketing the range of SDs for our time slices, see Table 1 and the discussion below (Figure 5). Considering the ranges of n and σ in our study, the estimation of σ_T indicates that the precision for the δ^{18}O SD is better than 0.1‰ for all time slices (at a 90% level of confidence), that increasing the number of individual measurements would not substantially increase the total precision in our description of the population, and that the number of individual measurements utilized is sufficient to describe the population within an acceptable degree of accuracy (Figure 5).

4. Results from Individual *N. dutertrei* δ^{18}O Measurements Over the Last 50 ka

4.1. Distribution of Individual *N. dutertrei* δ^{18}O Measurements

[15] Individual *N. dutertrei* δ^{18}O results were compared to downcore measurements using 2 to 3 specimens in Figure 6a (see auxiliary material).[1] The individual δ^{18}O data revealed a wide range in single test measurements for all time slices (Figure 6a and Table 1). Histograms of the δ^{18}O distribution indicated that all individual δ^{18}O values roughly followed a Gaussian distribution, even if some bimodality is apparent from δ^{18}O measurements in the early LGM and Heinrich event 4 (H4) time slices (Figure 6b). For the early LGM, one explanation for the apparent bimodality is that this time slice was derived from a subsampling of 4 sedimentary intervals distant by up to 9 cm in the sedimentary sequence (Table 1). The H4 also showed some bimodality even if all of the individual measurements were performed on the same 1-cm-wide sedimentary interval, with two apparent modes of 0.5‰ difference in δ^{18}O (Figure 6b). We performed a Shapiro-Wilk

[1] Auxiliary materials are available at ftp://ftp.agu.org/apend/pa/2008pa001701.

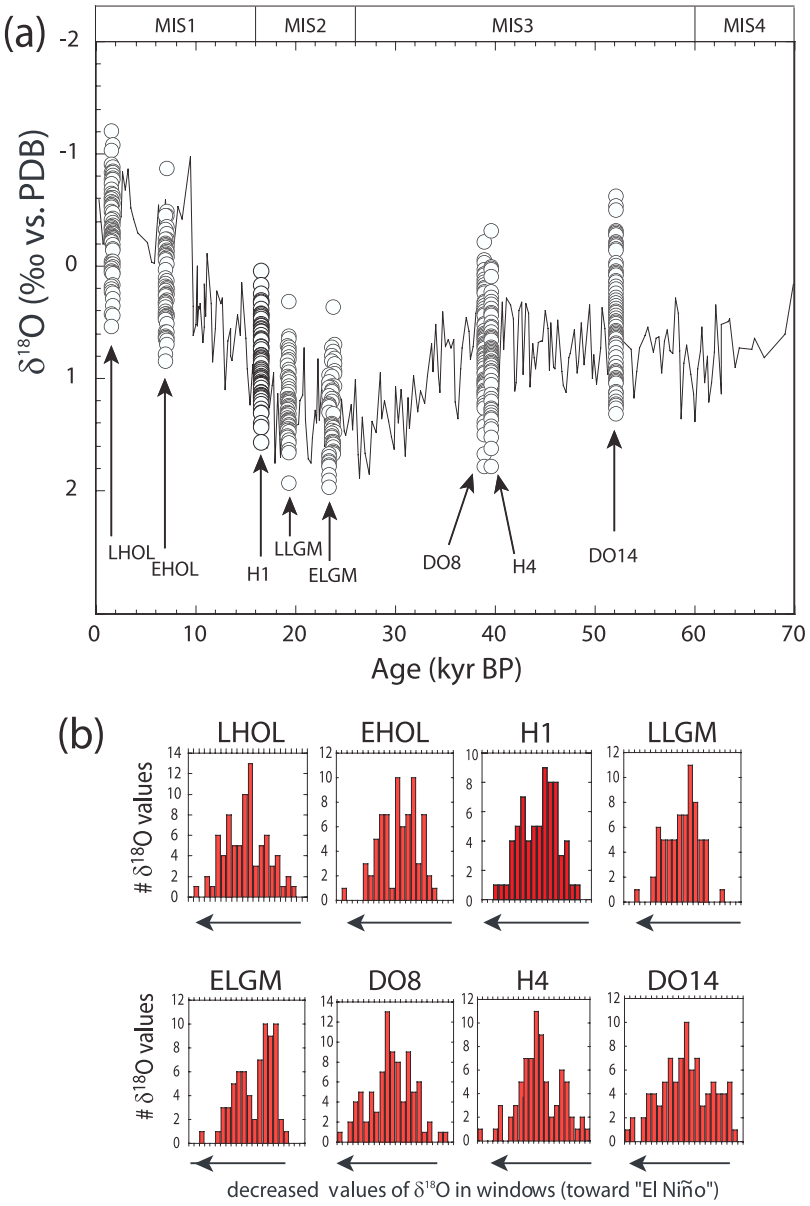

Figure 6. (a) Multiple-specimen (curve) and individual specimen (circles) δ^{18}O measurements performed on *N. dutertrei*. Marine isotopic stages are labeled at the top of the plot. (b) Histograms representing the number of individual *N. dutertrei* δ^{18}O values. Each vertical bar corresponds to the number of results falling within a 0.1‰ δ^{18}O window; each time slice histogram width is 2.2‰ (i.e., 22 windows are shown).

test, to test a null hypothesis of a univariate normal distribution. The probability that the H4 δ^{18}O data followed a normal distribution was only 52%, indicating that part of the SD linked to step changes in the background climate may have occurred during this time period. In the following discussion we assume that individual *N. dutertrei* δ^{18}O measurements follow a Gaussian distribution in the statistical tests performed on the entire data sets.

[16] The total range in individual δ^{18}O measurements varied between ~1.6‰ and ~2‰ for MIS2 and MIS3, respectively, while Holocene values had an intermediate range (~1.7 to 1.75‰ (Figure 6a and Table 1)). These ranges corresponded to temperature ranges of up to 10°C, likely representing a mixture of seasonal changes in the hydrologic patterns, vertical distribution of *N. dutertrei* depth habitat, and interannual temperature variability linked to ENSO.

[17] The modern seasonal amplitude of the expected δ^{18}O of calcite within the thermocline is larger than 1‰, indicating that more than half of *N. dutertrei* δ^{18}O scattering can potentially be explained by seasonal variability only. However, we note that more than half of this seasonal variability is only due to December and January (Figures 2a and 2b). Without December and January, the seasonality is reduced to 0.4‰. Furthermore, sediment traps from the Panama Basin have indicated that more than 75% of *N. dutertrei* fluxes occur between February and May [*Thunell et al.*,

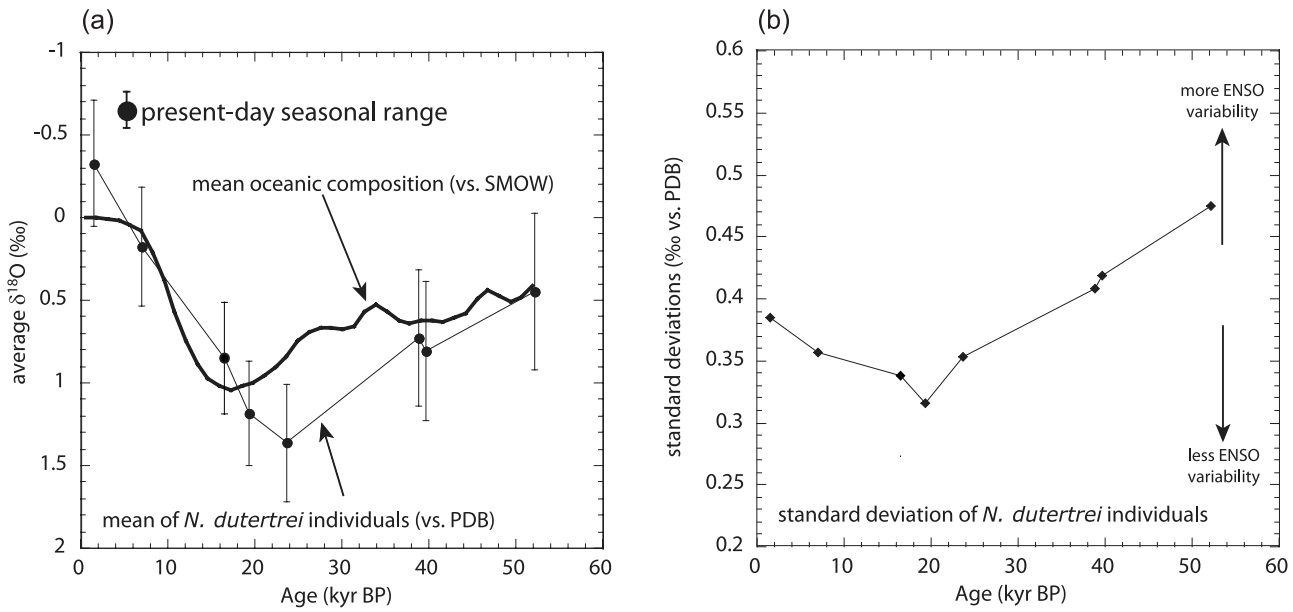

Figure 7. (a) Temporal variations of the mean *N. dutertrei* $\delta^{18}O$ individual measurements at each time slice (thin black curve and black dots) as compared to variations in the mean oceanic $\delta^{18}O_{sw}$ (thick black curve). (b) Temporal variations of the standard deviation of *N. dutertrei* $\delta^{18}O$ individual measurements at each time slice.

1983]. Over this winter-spring time period, the impact of the seasonal cycle on *N. dutertrei* isotopes is greatly reduced compared to the whole temperature and salinity range occurring over a full seasonal cycle. Some uncertainties inherent to paleoceanographic reconstruction are linked to past changes in thermocline seasonality that have influenced the *N. dutertrei* isotopes. However, seasonal changes in the thermocline have likely played a secondary role on the scattering of the single specimen analyses since the net seasonal effect may be of a lower amplitude than the net interannual effect (Figure 3). The method we applied cannot deconvolve changes in seasonal and interannual thermocline variability in the past. Yet, thermocline variability linked to ENSO at the core location is likely to be more sensitive than thermocline variability linked to seasonal changes over the February–May time interval (i.e., when *N. dutertrei* is most abundant).

[18] The vertical distribution of *N. dutertrei* indicates that this species lives from the top to the base of the thermocline, with a corresponding increase in $\delta^{18}O$ (Figure 2d). Approximately half of the whole inventory of *N. dutertrei* is found between 30 and 50 m, where a $\delta^{18}O$ gradient of 1‰ is recorded and reflects the sharp temperature gradient (Figure 2d). It indicates that more than half of the range of individual $\delta^{18}O$ measurements can be explained by the vertical distribution of foraminifera within the water column. However, the inventory shown in Figure 2d likely integrates the entire *N. dutertrei* size spectrum, with, as an example, juveniles living in the upper part of the water column. Some increases in *N. dutertrei* $\delta^{18}O$ have also been observed for increasing test size [*Bouvier-Soumagnac and Duplessy*, 1985], suggesting that selecting only large *N. dutertrei* restricts the biases linked to scattering in the habitat depth. The Mg/Ca distribution within shells seems to confirm that *N. dutertrei* form the inner parts of test walls in surface waters before migrating downward and adding the final outer calcite crust [*Sadekov et al.*, 2005]. Since we selected large tests, we may have reduced the scattering in $\delta^{18}O$ due to the vertical distribution of *N. dutertrei* in the water column. Given that the amplitude of *N. dutertrei* $\delta^{18}O$ ranges for all time slices were higher than the effects we would have expected from the influence of seasonal variations and the vertical distribution within the water column, we conclude that ENSO has a significant impact on the full *N. dutertrei* $\delta^{18}O$ ranges. Although seasonality and depth habitat contributions cannot be ruled out, in the following discussion it is assumed that changes in *N. dutertrei* in past time slices are primarily driven by ENSO variability, with only secondary contributions from seasonal and depth effects.

4.2. Temporal Changes in the Mean and the SD of Individual *N. dutertrei* $\delta^{18}O$ Measurements

[19] Temporal variations in the mean for individual $\delta^{18}O$ measurements in each time slice were compared to the mean oceanic $\delta^{18}O_{sw}$ in Figure 7a. Between the late Holocene and the LGM, the mean *N. dutertrei* $\delta^{18}O$ values increase is larger than the mean oceanic $\delta^{18}O_{sw}$ increase because of variations in continental ice volume (Figure 7a), indicating decreased temperature or increased salinity in EEP undercurrent hydrologic parameters that ultimately impact the thermocline at the MD02-2529 core location [*Pena et al.*, 2008].

[20] At the millennial timescale, mean *N. dutertrei* $\delta^{18}O$ values are nearly identical between, for example, Heinrich event 4 (H4) and the following DO event 8. Since the EEP undercurrent may integrate a mixture of surface waters originating from both the North and South Pacific subtropical gyres [*Gu and Philander*, 1997], and assuming temperature

Table 2. *F* Test Matrix Giving the Probability That Any Two Time Slices Have Different Variance Estimates[a]

	LHOL	EHOL	H1	LLGM	ELGM	DO8	H4	DO14
LHOL	0	-	-	-	-	-	-	-
EHOL	48.24	0	-	-	-	-	-	-
H1	70.25	31.08	0	-	-	-	-	-
LLGM	90.34	68.77	45.27	0	-	-	-	-
ELGM	52.90	6.15	25.22	64.69	0	-	-	-
DO8	40.92	76.01	88.13	97.09	78.68	0	-	-
H4	55.04	82.83	91.76	98.09	84.81	19.13	0	-
DO14	94.21	98.65	99.51	99.94	98.84	83.74	72.80	0

[a]Probability is given in percent.

changes only, the temperature averaged over the whole subtropical Pacific may not dramatically change in response to abrupt climatic changes occurring during the MIS3.

[21] Assuming that the SD reflects the population variability for each time slice, we calculated the temporal changes in the SD of individual measurements performed on *N. dutertrei* in order to assess how thermocline variability evolved over the last 50 ka (Figure 7b). Long-term trends in thermocline variability are recorded, with a decreasing SD tendency from the late Holocene to the late LGM, followed by a long-term increase until the highest variability is reached in the early MIS3 time interval that corresponds to the Dansgaard-Oeschger 14 interstadial (Figure 7b).

5. Past ENSO Activity Deduced From EEP Thermocline Variability

[22] We now focus on temporal variations in thermocline instability as deduced from changes in SD likely reflecting past changes in ENSO activity. A matrix of Fischer *F* tests values is provided, giving the probability that thin discreet time slices are statistically different (Table 2). Our results suggest that, with the exception of samples with highest and lowest SD, no statistically significant ENSO changes have occurred over the time period studied. For example, the late LGM $\delta^{18}O$ data set is of lower variability than MIS3 time slices within the 95% confidence level, the Dansgaard-Oeschger interstadial 14 time slice is of higher variability than the late LGM time slice with a probability higher than 99.9%, and the early Holocene and early LGM time slices are identical within a 90% confidence level (Table 2).

[23] We now compare variations in calculated SDs to climate records and modeling outputs proposed to influence ENSO in the literature (Figure 8).

5.1. ENSO Activity Changes During the Holocene

[24] According to Holocene SD values the ENSO activity during the early Holocene was not statistically lower than late Holocene ENSO activity (Figure 8), with a probability that late Holocene SD is larger than early Holocene of 48% (Table 2). It implies that our data reflect no ENSO increase between the two time slices. This result contrasts with previous studies based on modeling experiments [*Liu et al.*, 2000; *Otto-Bliesner et al.*, 2003, 2006; *Zheng et al.*, 2008; *Brown et al.*, 2008; *Emile-Geay et al.*, 2007], and paleo-ENSO reconstructions based on corals [*Tudhope et al.*, 2001; *McGregor and Gagan*, 2004], on Ecuador sediments [*Moy et al.*, 2002; *Conroy et al.*, 2008], on marine and terrestrial archives in circum-Pacific regions [*Donders et al.*, 2008] and on individual measurements of surface-dwelling planktonic foraminifera in the EEP cold tongue [*Koutavas et al.*, 2006].

[25] By using data presented in the study of *Koutavas et al.* [2006], the probability that SD changes recorded between early Holocene and late Holocene data sets are significant is higher than 99.9%, suggesting that the cold tongue may be more sensitive to changes in ENSO than the EEP thermocline. Also, one should consider that the data from *Koutavas et al.* [2006] are based on *G. ruber* and may contain a superimposed signal linked to seasonality changes. In the cold tongue area, seasonal changes in temperature and salinity are higher than in the EEP thermocline. Therefore, we cannot rule out that the method used by *Koutavas et al.* [2006] was more subject to variations in the seasonal cycle (for example, see *Lorenz et al.* [2006] for seasonality change in Holocene sea surface temperatures and *Braconnot et al.* [2007a, 2007b] for recent diagnostics for change in the low-latitude hydrologic cycle during the mid-Holocene).

[26] According to modeling by *Liu et al.* [2000], two mechanisms may have contributed to a reduction in ENSO variability from the early to the mid-Holocene. First, an intensification in the Asian summer monsoon during the boreal summer [*Yuan et al.*, 2004] leads to an intensified deep convection in Asia, increased easterly trade winds and a strengthening in the Walker circulation, helping to decrease ENSO activity [*Liu et al.*, 2000; *Zheng et al.*, 2008]. Second, a substantial increase in EEP thermocline temperatures (by $\sim$0.2°C during the mid-Holocene) may have reduced the ability of upwelling waters to influence surface temperatures, and thereby helped to suppress ENSO [*Liu et al.*, 2000]. Nevertheless, such a small thermocline temperature shift is hard to detect in paleoclimate records, and no significant thermocline temperature changes were recorded in the EEP during the Holocene [*Pena et al.*, 2008].

[27] On the other hand, other studies based on narrow time windows reported stronger ENSO variability during the early to mid-Holocene than for present-day conditions [*McCulloch et al.*, 1996; *Corrège et al.*, 2000; *Carré et al.*, 2005]. Taken at face value, the results mentioned above and the lack of a clear Holocene SD evolution in our data set stresses the need for obtaining better time coverage with these methods.

5.2. ENSO Changes Between the Holocene and the Last Glacial Period

[28] Our data suggest marginally reduced ENSO activity during the LGM as compared to the Holocene, with the late LGM time slice apparently being a period with lowest ENSO activity (Figure 8). Since no fossil corals are avail-

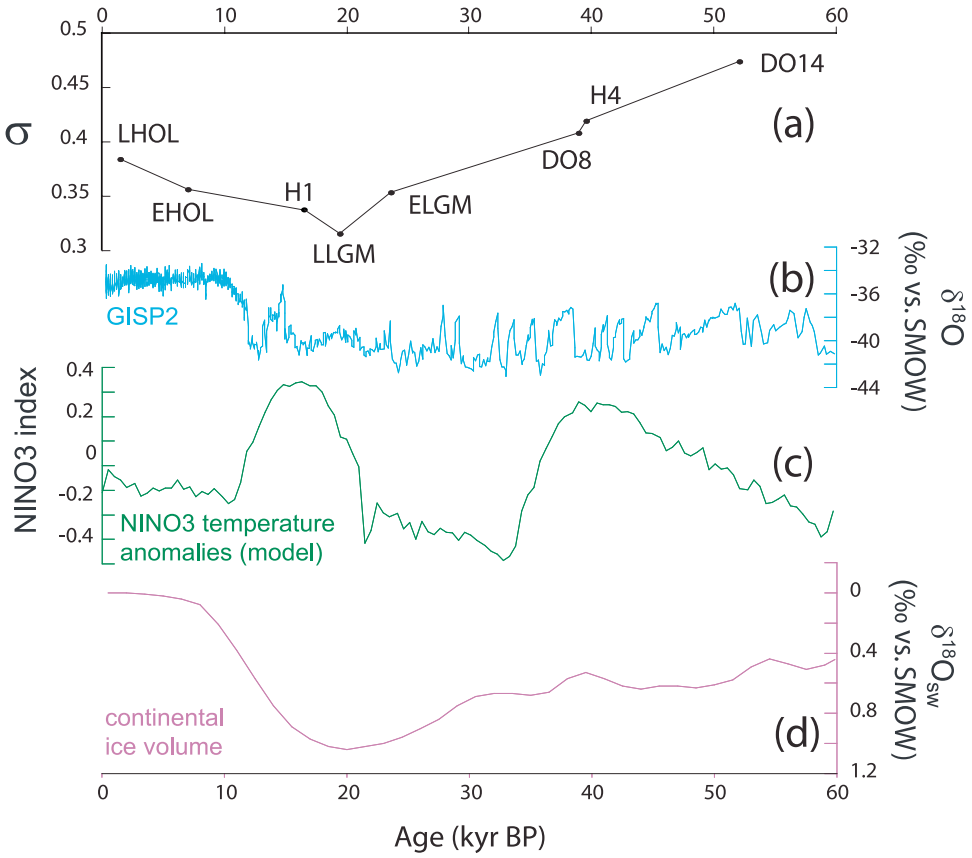

Figure 8. (a) Comparison of temporal changes in ENSO variability derived from the δ^{18}O SD to reference climatic curves: (b) abrupt climatic changes in the North Atlantic area as recorded by GISP2 δ^{18}O (a proxy for surface air temperature above Greenland) [*Stuiver and Grootes*, 2000], (c) the NINO3 index derived from the Zebiak-Cane ENSO model [*Zebiak and Cane*, 1987] forced by changes in orbital parameters [*Clement et al.*, 1999], and (d) variations in mean oceanic δ^{18}O (a proxy for variations in continental ice volume) [*Waelbroeck et al.*, 2002].

able for the LGM, little is known regarding ENSO activity at this time, even if corals from the last glacial period reported reduced ENSO activity [*Tudhope et al.*, 2001].

[29] Paleo-ENSO simulations under glacial boundary conditions lead to antagonist results for ENSO activity during the LGM. While some models report increased ENSO activity during the LGM [*Otto-Bliesner et al.*, 2003; *An et al.*, 2004; *Peltier and Solheim*, 2004], other models report decreased ENSO activity [*Otto-Bliesner et al.*, 2006]. One recent compilation for simulated changes in ENSO characteristics at 21 ka B.P. indicates that only two models recorded significant changes in ENSO variability but with opposite results [*Zheng et al.*, 2008]. The model with decreased ENSO activity was the same as that presented by *Otto-Bliesner et al.* [2006], namely, the CCSM3 model.

[30] In marine sediments, reconstructions of the background hydrologic state during the LGM remain controversial, displaying either El Niño–like [*Koutavas et al.*, 2002] or La Niña–like [*Martínez et al.*, 2003] oceanic states. These divergent conclusions are based on dissimilarities in amplitude of SST rise over the deglaciation that can be explained by the different SST estimation methods used in these studies (see discussion by *Rosenthal and Broccoli* [2004]). The marginally lower SD that we report for the LGM suggests reduced ENSO activity (Figure 8), but cannot distinguish potential changes in the mean climate state toward ENSO-like configurations. Moreover, our hypothesis for reduced LGM ENSO is based only on two time slices from the LGM, and the *F* tests results indicate that the reduced LGM variance does not attain 95% significance in all cases (Table 2). More studies from corals or from single-specimen foraminifera δ^{18}O could help to confirm this hypothesis.

5.3. ENSO Changes During the MIS3

[31] According to our data set, ENSO activity did not respond to rapid climate shifts such as Heinrich events and DO interstadials, especially when results from H4 and DO8 are compared (Figure 8). This result reinforces the idea that ENSO variability was not affected by rapid climate changes over the last glacial period [*Leduc et al.*, 2009]. The highest ENSO activity was found at the beginning of the MIS3, during DO interstadial 14 (Figure 8). Therefore some evidence exists that ENSO activity was higher during the last glacial period than today. Additionally, the long-term evolution from higher ENSO variability at the beginning of

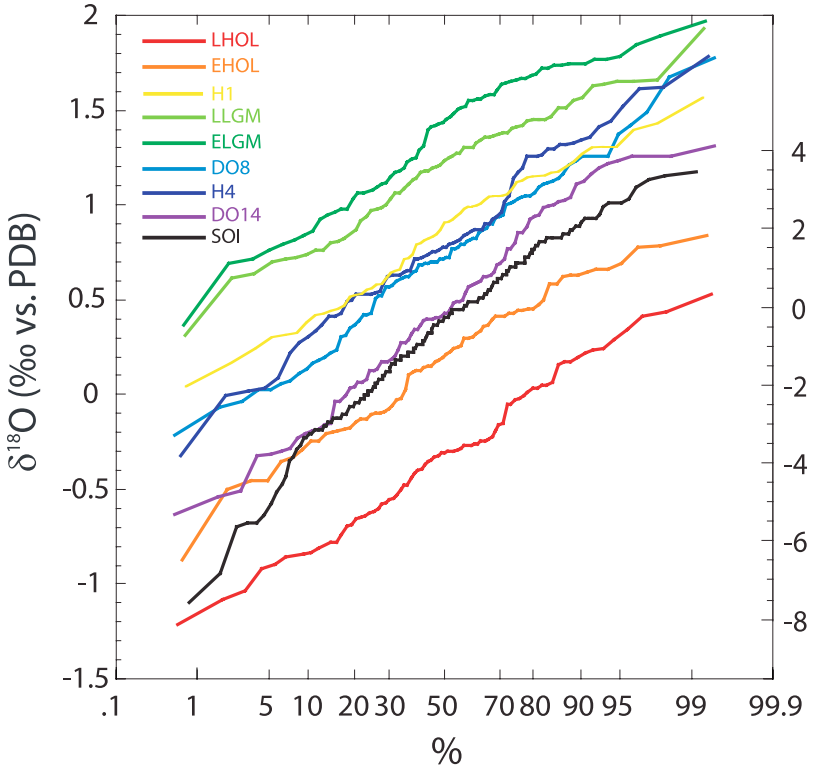

Figure 9. Cumulative distribution curves (CDC) of individual *N. dutertrei* δ^{18}O measurements for each time slice. Refer to Figure 10 in order to interpret the shape of each CDC and for the mechanism needed to compare time slices. SOI data for the last 20 years are shown for a comparison of symmetry in modern-day ENSO variability.

the MIS3 does not indicate a clear influence of continental ice volume on ENSO, since the highest variability was found during the last glacial period and not the Holocene (Figure 8).

[32] During periods of abrupt climate changes such as those for MIS3, the bioturbation of deep-sea sediments by benthic organisms may have artificially enhanced the scattering of samples by reworking foraminifera tests across sharp transitions. In the case of MD02-2529, bioturbation may have had little impact on the distribution of single δ^{18}O measurements performed on *N. dutertrei* for two reasons. First, the difference between the mean for δ^{18}O measurements in the H4 and DO8 samples is two to three times lower than the difference between the two modes of the H4 bimodal sample (Figure 6 and Table 1), indicating that the incursion of foraminifera from the DO8 to the H4 sedimentary interval through bioturbation is unlikely to produce the bimodality observed in the H4 sample. Second, the δ^{18}O measured on *G. ruber* (from 5 to 6 individuals) is clearly marked during this time period by a very sharp transition of more than 1‰ (Figure 4), occurring over a 4 cm sediment depth interval, and bracketing the *N. dutertrei* H4 and DO8 time slices. Therefore we believe that bioturbation exerts no significant increase on the SD because of sediment mixing during sharp transitions over the last glacial period.

[33] Since variations in precession modulate the asymmetric solar heating North and South of the equator in the EEP, it has been suggested that variations in precession can modulate ENSO at orbital timescales [*Clement et al.*, 1999]. Our reconstruction for past ENSO activity does not seem to correspond to Nino3 model output [*Clement et al.*, 1999] (Figure 8), again suggesting that under glacial boundary conditions feedbacks other than insolation may operate and modulate ENSO activity changes.

[34] Low-latitude speleothem records indicate that the ITCZ latitudinal migrations were modulated at both millennial and precessional timescales (for example, see *Yuan et al.* [2004] and *Wang et al.* [2007] among others). Given that our data show that neither millennial-scale nor orbital-scale climatic changes may have modulated ENSO activity changes recorded during the last glacial period, we suggest that paleorecords which report southward shifts for the mean latitudinal position of the ITCZ should potentially not be interpreted as reflecting more intense El Niño conditions [*Leduc et al.*, 2009].

5.4. Past Changes in ENSO Asymmetry

[35] Modern-day ENSO variability involves more El Niño warm phases than La Niña cold phases [*An and Jin*, 2004], a feature captured in climatic models [*Park et al.*, 2009]. Nevertheless, modeling results of past ENSO variability suggest that a relationship exists between the number of warm events, the number of cold events and the amplitude of these events, pointing to a rough symmetry involved in the oscillatory nature of ENSO [*Clement et al.*, 1999]. Similar rough symmetry for different mean states of ENSO activity have been found in modeling studies at 6 ka B.P. and for the

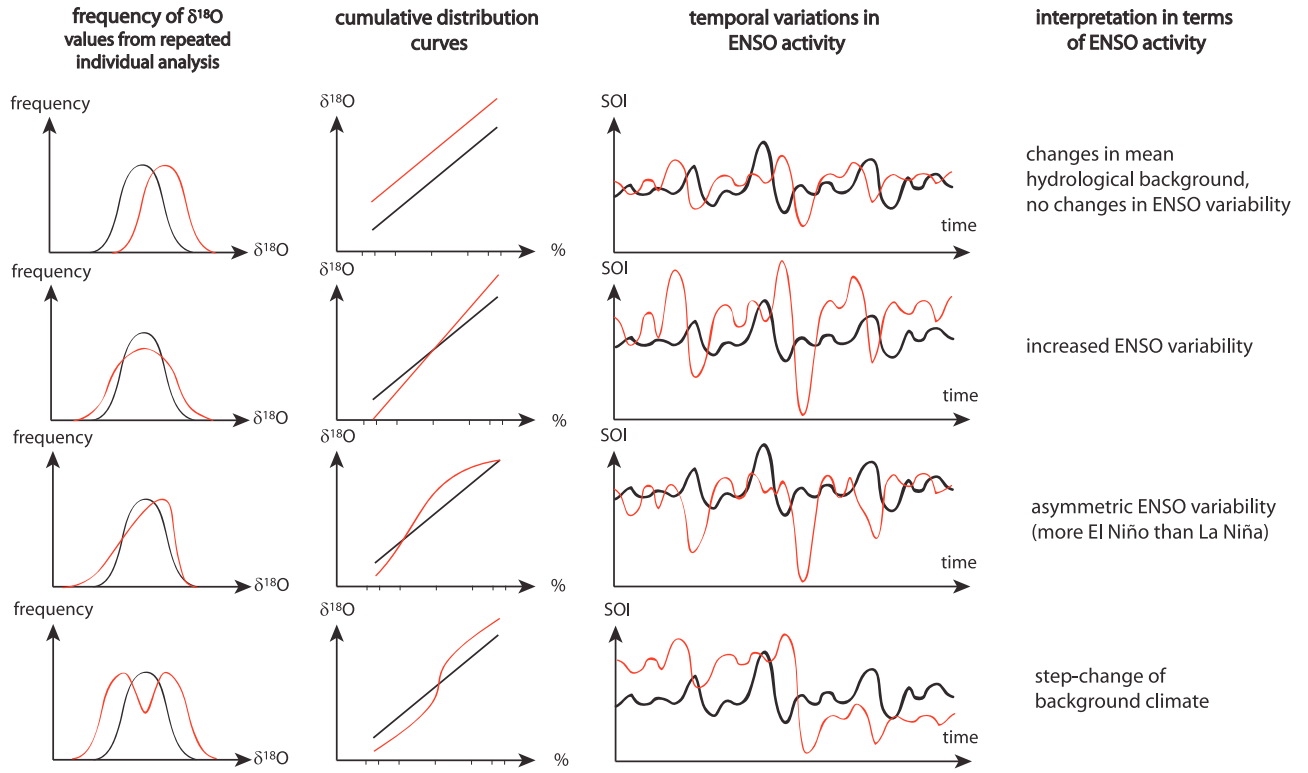

Figure 10. Conceptual model for interpreting the shape of cumulative distribution curves (CDC) in terms of ENSO variability (see Figure 9).

LGM [*Otto-Bliesner et al.*, 2006]. Theoretically, the method developed in this study has the potential to detect ENSO asymmetry by examining the asymmetry in the distribution of δ^{18}O measurements. We tentatively investigate with our data sets if any skewness is recorded in repeated *N. dutertrei* δ^{18}O measurements that can be interpreted in terms of ENSO asymmetry.

[36] To compare the isotopic distribution spectra of all time slices within the same graphic, we adopted the strategy of *Billups and Spero* [1996] by plotting the isotopic data as a function of cumulative distribution (Figure 9; see also Figure 10 for an illustration of this strategy). The late Holocene cumulative distribution curves (CDC) that may have recorded the most recent ENSO activity is relatively straight (Figure 9). Assuming that the late Holocene time slice faithfully represents the modern-day ENSO activity as captured by our method, the sensitivity of the method seems not to be sufficient enough to detect any degree of ENSO asymmetry lower or equal to today's asymmetry.

[37] At first sight, the CDC derived from *N. dutertrei* repeated analysis seem to be roughly linear for all time slices (Figure 9), suggesting that some strong asymmetrical ENSO variability in the past is unlikely to have been captured by our method. Further scrutinization of CDCs may suggest smooth ENSO asymmetry revealed by smooth CDC curvatures seen in the LGM time slices, likely revealing potential skewness in ENSO activity in these data sets. Despite the potential ENSO skewness increases for the LGM time slices, the CDCs may suggest that drastic changes in ENSO asymmetry are rather unlikely for the time slices studied. If the oscillatory nature of ENSO persisted in the past with more or less frequent ENSO events that were associated with more or less amplitude in ENSO events, as CDCs suggest at first order, then the terminology of "El Niño–like" or "La Niña–like" should be used with care since these terms could potentially refer to changes in the climate mean state rather than to asymmetrical responses in ENSO [*Rosenthal and Broccoli*, 2004].

6. Conclusions

[38] In this study we reconstructed past ENSO changes by extracting the entire thermocline variability spectra in the EEP at targeted time slices, through repeated intrasample isotopic analyses performed on individual planktonic foraminifera. The calibration of this method by comparing core top sedimentary results to modern-day planktonic foraminifera ecological behavior and hydrologic variability demonstrates that the method is powerful for reconstructing the past hydrologic variability spectra for different time slices, and that it minimizes the impact of seasonality that may have generated additional variability in the paleo-ENSO sedimentary records formerly published.

[39] We found some indications that long-term changes in ENSO activity occurred over the last 50 ka with a minimum and maximum in ENSO activity occurring during the LGM and the early MIS3 (DO14), respectively, although the magnitude was small and often not statistically significant. The findings provide new benchmarks for paleo-ENSO modeling analyses, especially for the LGM epoch for which

no ENSO activity records are yet available. The results also indicate that higher ENSO activity may have occurred during the last glacial period, a result that should be tested by modeling experiments.

[40] Given the rather small amplitude of reconstructed ENSO changes, we conclude that ENSO dynamics remained active throughout the last 50 ka. This does not support a role for ENSO as a primary driver of climatic variability on a global scale, nor indicate a drastic impact in its evolution in response to climate changes. Although our approach did not allow us to reconstruct ENSO with a time resolution comparable to other paleoclimatic reconstruction methods, we hope that this work will foster new studies for past ENSO changes with a special emphasis on variations in seasonality, a parameter that should be circumvented to accurately reconstruct ENSO.

[41] **Acknowledgments.** We thank Corinne Sonzogni for her help with the isotopic analysis, Tom Koutavas for his interest and remarks, two anonymous reviewers for constructive comments, and Jerry Dickens for reviewing the manuscript. This work was funded by the CNRS LEFE-EVE-MISLOLA program.

References

An, S.-I., and F.-F. Jin (2004), Nonlinearity and asymmetry of ENSO, *J. Clim.*, *17*, 2399–2412, doi:10.1175/1520-0442(2004)017<2399:NAAOE>2.0.CO;2.

An, S.-I., A. Timmermann, L. Bejarano, F.-F. Jin, F. Justino, Z. Liu, and A. W. Tudhope (2004), Modeling evidence for enhanced El Niño–Southern Oscillation amplitude during the Last Glacial Maximum, *Paleoceanography*, *19*, PA4009, doi:10.1029/2004PA001020.

Bard, E. (2001), Paleoceanographic implications of the difference in deep-sea sediment mixing between large and fine particles, *Paleoceanography*, *16*(3), 235–239, doi:10.1029/2000PA000537.

Benway, H. M., and A. C. Mix (2004), Oxygen isotopes, upper-ocean salinity, and precipitation sources in the eastern tropical Pacific, *Earth Planet. Sci. Lett.*, *224*, 493–507, doi:10.1016/j.epsl.2004.05.014.

Billups, K., and H. J. Spero (1996), Reconstructing the stable isotope geochemistry and paleotemperatures of the equatorial Atlantic during the last 150000 years: Results from individual foraminifera, *Paleoceanography*, *11*(2), 217–238, doi:10.1029/95PA03773.

Bouvier-Soumagnac, Y., and J.-C. Duplessy (1985), Carbon and oxygen isotopic composition of planktonic foraminifera from laboratory culture, plankton tows and recent sediments: Implications for the reconstruction of paleoclimatic conditions and of the global carbon cycle, *J. Foraminiferal Res.*, *15*, 302–320.

Braconnot, P., et al. (2007a), Results of PMIP2 coupled simulations of the mid-Holocene and Last Glacial Maximum—Part 1: Experiments and large-scale features, *Clim. Past*, *3*, 261–277.

Braconnot, P., et al. (2007b), Results of PMIP2 coupled simulations of the mid-Holocene and Last Glacial Maximum—Part 2: Feedbacks with emphasis on the location of the ITCZ and mid- and high latitudes heat budget, *Clim. Past*, *3*, 279–296.

Brown, J., A. W. Tudhope, M. Collins, and H. V. McGregor (2008), Mid-Holocene ENSO: Issues in quantitative model-proxy data comparisons, *Paleoceanography*, *23*, PA3202, doi:10.1029/2007PA001512.

Cane, M. A. (1998), A role for the tropical Pacific, *Science*, *282*, 59–61, doi:10.1126/science.282.5386.59.

Cane, M. A. (2005), The evolution of El Niño, past and future, *Earth Planet. Sci. Lett.*, *230*, 227–240, doi:10.1016/j.epsl.2004.12.003.

Carré, M., I. Bentaleb, M. Fontugne, and D. Lavallée (2005), Strong El Niño events during the early Holocene: Stable isotope evidence from Peruvian sea-shells, *Holocene*, *15*(1), 42–47, doi:10.1191/0959683605h1782rp.

Clement, A. C., R. Seager, and M. A. Cane (1999), Orbital control on El Niño/Southern Oscillation and the tropical climate, *Paleoceanography*, *14*(4), 441–456, doi:10.1029/1999PA900013.

Clement, M. A., M. A. Cane, and R. Seager (2001), An orbitally driven tropical source for abrupt climate change, *J. Clim.*, *14*, 2369–2375, doi:10.1175/1520-0442(2001)014<2369:AODTSF>2.0.CO;2.

Cobb, K. M., C. D. Charles, H. Cheng, and R. L. Edwards (2003), El Niño/Southern Oscillation and tropical Pacific climate during the last millennium, *Nature*, *424*, 271–276, doi:10.1038/nature01779.

Conkright, M. E., R. A. Locarnini, H. E. Garcia, T. O'Brien, T. P. Boyer, C. Stephens, and J. I. Antonov (2002), World Ocean Atlas 2001: Objective analyses, data statistics, and figures CD-ROM documentation, *Internal Rep. 17*, 17 pp., NOAA, Silver Spring, Md.

Conroy, J. L., J. T. Overpeck, J. E. Cole, T. M. Shanahan, and M. Steinitz-Kannan (2008), Holocene changes in eastern tropical Pacific climate inferred from a Galápagos lake sediment record, *Quat. Sci. Rev.*, *27*, 1166–1180, doi:10.1016/j.quascirev.2008.02.015.

Corrège, T., T. Delcroix, J. Rècy, W. Beck, G. Cabioch, and F. Le Cornec (2000), Evidence for stronger El Niño-Southern Oscillation (ENSO) events in a mid-Holocene massive coral, *Paleoceanography*, *15*(4), 465–470, doi:10.1029/1999PA000409.

Curry, W. B., R. C. Thunell, and S. Honjo (1983), Seasonal changes in the isotopic composition of planktonic foraminifera collected in Panama Basin sediment traps, *Earth Planet. Sci. Lett.*, *64*, 33–43, doi:10.1016/0012-821X(83)90050-X.

Denton, G. H., R. B. Alley, G. C. Comer, and W. S. Broecker (2005), The role of seasonality in abrupt climate change, *Quat. Sci. Rev.*, *24*, 1159–1182, doi:10.1016/j.quascirev.2004.12.002.

Donders, T. H., F. Wagner-Cremer, and H. Visscher (2008), Integration of proxy data and model scenarios for the mid-Holocene onset of modern ENSO variability, *Quat. Sci. Rev.*, *27*, 571–579, doi:10.1016/j.quascirev.2007.11.010.

Emile-Geay, J., M. Cane, R. Seager, A. Kaplan, and P. Almasi (2007), El Niño as a mediator of the solar influence on climate, *Paleoceanography*, *22*, PA3210, doi:10.1029/2006PA001304.

Fairbanks, R. G., and P. H. Wiebe (1980), Foraminifera and chlorophyll maximum: Vertical distribution, seasonal succession, and paleoceanographic significance, *Science*, *209*, 1524–1526, doi:10.1126/science.209.4464.1524.

Fairbanks, R. G., M. Sverdlove, R. Free, P. H. Wiebe, and A. W. H. Bé (1982), Vertical distribution and isotopic fractionation of living planktonic foraminifera from the Panama Basin, *Nature*, *298*, 841–844, doi:10.1038/298841a0.

Fairbanks, R. G., M. N. Evans, J. L. Rubenstone, R. A. Mortlock, K. Broad, M. D. Moore, and C. D. Charles (1997), Evaluating climate indices and their geochemical proxies measured in corals, *Coral Reefs*, *16*, S93–S100, doi:10.1007/s003380050245.

Faul, K. L., A. C. Ravelo, and M. D. Delaney (2000), Reconstructions of upwelling, productivity, and photic zone depth in the eastern equatorial Pacific Ocean using planktonic foraminifera stable isotopes and abundances, *J. Foraminiferal Res.*, *30*, 110–125, doi:10.2113/0300110.

Fiedler, P. C. (2002), The annual cycle and biological effect of the Costa Rica Dome, *Deep Sea Res., Part I*, *49*, 321–338, doi:10.1016/S0967-0637(01)00057-7.

Fiedler, P. C., and L. D. Talley (2006), Hydrography of the eastern tropical Pacific: A review, *Prog. Oceanogr.*, *69*, 143–180, doi:10.1016/j.pocean.2006.03.008.

Flückiger, J., R. Knutti, J. W. C. White, and H. Renssen (2008), Modeled seasonality of glacial abrupt climate change, *Clim. Dyn.*, *31*, 633–645, doi:10.1007/s00382-008-0373-y.

Grelaud, M., L. Beaufort, S. Cuven, and N. Buchet (2009), Glacial to interglacial primary production and El Niño–Southern Oscillation dynamics inferred from coccolithophores of the Santa Barbara Basin, *Paleoceanography*, *24*, PA1203, doi:10.1029/2007PA001578.

Gu, D., and S. G. H. Philander (1997), Interdecadal climate fluctuations that depend on exchanges between the tropics and extratropics, *Science*, *275*, 805–807, doi:10.1126/science.275.5301.805.

Koutavas, A., and J. Lynch-Stieglitz (2003), Glacial-interglacial dynamics of the eastern equatorial Pacific cold tongue-Intertropical Convergence Zone system reconstructed from oxygen isotope records, *Paleoceanography*, *18*(4), 1089, doi:10.1029/2003PA000894.

Koutavas, A., J. Lynch-Stieglitz, T. Marchitto, and J. Sachs (2002), El Niño-like pattern in ice age tropical Pacific sea surface temperature, *Science*, *297*, 226–230, doi:10.1126/science.1072376.

Koutavas, A., P. B. deMenocal, G. C. Olive, and J. Lynch-Stieglitz (2006), Mid-Holocene El Niño–Southern Oscillation (ENSO) attenuation revealed by individual foraminifera in

eastern tropical Pacific sediments, *Geology*, *34*, 993–996, doi:10.1130/G22810A.1.

Leduc, G., L. Vidal, K. Tachikawa, F. Rostek, C. Sonzogni, L. Beaufort, and E. Bard (2007), Moisture transport across Central America as a positive feedback for abrupt climatic feedback on abrupt climatic changes, *Nature*, *445*, 908–911, doi:10.1038/nature05578.

Leduc, G., L. Vidal, K. Tachikawa, and E. Bard (2009), ITCZ rather than ENSO signature for abrupt climate changes across the tropical Pacific?, *Quat. Res.*, *72*, 123–131, doi:10.1016/j.yqres.2009.03.006.

Linsley, B. K., R. B. Dunbar, G. M. Wellington, and D. A. Mucciarone (1994), A coral-based reconstruction of the Intertropical Convergence Zone variability over Central America since 1707, *J. Geophys. Res.*, *99*(C5), 9977–9994, doi:10.1029/94JC00360.

Liu, Z., and M. Alexander (2007), Atmospheric bridge, oceanic tunnel, and global climatic teleconnections, *Rev. Geophys.*, *45*, RG2005, doi:10.1029/2005RG000172.

Liu, Z., J. Kutzbach, and L. Wu (2000), Modeling climate shift of El Nino variability in the Holocene, *Geophys. Res. Lett.*, *27*(15), 2265–2268, doi:10.1029/2000GL011452.

Lorenz, S. J., J.-H. Kim, N. Rimbu, R. R. Schneider, and G. Lohmann (2006), Orbitally driven insolation forcing on Holocene climate trends: Evidence from alkenone data and climate modeling, *Paleoceanography*, *21*, PA1002, doi:10.1029/2005PA001152.

Martínez, I., L. Keigwin, T. T. Barrows, Y. Yokoyama, and J. Southon (2003), La Niña-like conditions in the eastern equatorial Pacific and a stronger Choco jet in the northern Andes during the last glaciation, *Paleoceanography*, *18*(2), 1033, doi:10.1029/2002PA000877.

McCulloch, M., G. Mortimer, T. Esat, L. Xianhua, B. Pillans, and J. Chappell (1996), High resolution windows into early Holocene climate: Sr/Ca coral records from the Huon peninsula, *Earth Planet. Sci. Lett.*, *138*, 169–178, doi:10.1016/0012-821X(95)00230-A.

McGregor, H. V., and M. K. Gagan (2004), Western Pacific coral δ^{18}O records of anomalous Holocene variability in the El Niño–Southern Oscillation, *Geophys. Res. Lett.*, *31*, L11204, doi:10.1029/2004GL019972.

Moy, C. M., G. O. Seltzer, D. T. Rodbell, and D. M. Anderson (2002), Variability of the El Niño/Southern Oscillation activity at millennial timescales during the Holocene epoch, *Nature*, *420*, 162–165, doi:10.1038/nature01194.

O'Neil, J. R., R. N. Clayton, and T. K. Mayeda (1969), Oxygen isotope fractionation in divalent metal carbonates, *J. Chem. Phys.*, *51*, 5547–5558.

Otto-Bliesner, B. L., E. C. Brady, S.-I. Shin, Z. Liu, and C. Shields (2003), Modeling El Niño and its tropical teleconnections during the last glacial-interglacial cycle, *Geophys. Res. Lett.*, *30*(23), 2198, doi:10.1029/2003GL018553.

Otto-Bliesner, B. L., E. C. Brady, G. Clauzet, R. Tomas, S. Levis, and Z. Kothavala (2006), Last Glacial Maximum and Holocene climate in CCSM3, *J. Clim.*, *19*, 2526–2544, doi:10.1175/JCLI3748.1.

Park, W., N. Keenlyside, M. Latif, A. Ströh, R. Redler, E. Roeckner, and G. Madec (2009), Tropical Pacific climate and its response to global warming in the Kiel climate model, *J. Clim.*, *22*, 71–92, doi:10.1175/2008JCLI2261.1.

Patrick, A., and R. C. Thunell (1997), Tropical Pacific sea surface temperature and upper water column thermal structure during the Last Glacial Maximum, *Paleoceanography*, *12*(5), 649–657, doi:10.1029/97PA01553.

Peltier, W. R., and L. P. Solheim (2004), The climate of the Earth at Last Glacial Maximum: Statistical equilibrium state and a mode of internal variability, *Quat. Sci. Rev.*, *23*, 335–357, doi:10.1016/j.quascirev.2003.07.003.

Pena, L. D., I. Cacho, P. Ferretti, and M. A. Hall (2008), El Niño–Southern Oscillation–like variability during glacial terminations and interlatitudinal teleconnections, *Paleoceanography*, *23*, PA3101, doi:10.1029/2008PA001620.

Rasmusson, E. M., and T. H. Carpenter (1982), Variations in tropical sea surface temperatures and surface wind fields associated with the Southern Oscillation/El Niño, *Mon. Weather Rev.*, *110*, 354–384, doi:10.1175/1520-0493(1982)110<0354:VITSST>2.0.CO;2.

Rein, B., A. Lückge, L. Reinhardt, F. Sirocko, A. Wolf, and W.-C. Dullo (2005), El Niño variability off Peru during the last 20000 years, *Paleoceanography*, *20*, PA4003, doi:10.1029/2004PA001099.

Rosenthal, Y., and A. J. Broccoli (2004), In search of paleo-ENSO, *Science*, *304*, 219–221, doi:10.1126/science.1095435.

Sadekov, A. Y., S. M. Eggins, and P. De Deckker (2005), Characterization of Mg/Ca distribution in planktonic foraminifera species by electron microprobe mapping, *Geochem. Geophys. Geosyst.*, *6*, Q12P06, doi:10.1029/2005GC000973.

Schiffelbein, P., and S. Hills (1984), Direct assessment of stable isotope variability in planktonic foraminifera populations, *Palaeogeogr. Palaeoclimatol. Palaeoecol.*, *48*, 197–213, doi:10.1016/0031-0182(84)90044-0.

Spero, H. J., K. M. Mielke, E. M. Kalve, D. W. Lea, and D. K. Pak (2003), Multispecies approach to reconstructing eastern equatorial Pacific thermocline hydrography during the past 360 kyr, *Paleoceanography*, *18*(1), 1022, doi:10.1029/2002PA000814.

Stott, L., C. Poulsen, S. Lund, and R. Thunell (2002), Super ENSO and global climate oscillations at millennial time scales, *Science*, *297*, 222–226, doi:10.1126/science.1071627.

Stuiver, M., and P. M. Grootes (2000), GISP2 oxygen isotope ratios, *Quat. Res.*, *53*, 277–284.

Thunell, R. C., W. B. Curry, and S. Honjo (1983), Seasonal variation in the flux of planktonic foraminifera: Time series sediment trap results from the Panama Basin, *Earth Planet. Sci. Lett.*, *64*, 44–55, doi:10.1016/0012-821X(83)90051-1.

Timm, O., A. Timmermann, A. Abe-Ouchi, F. Saito, and T. Segawa (2008), On the definition of seasons in paleoclimate simulations with orbital forcing, *Paleoceanography*, *23*, PA2221, doi:10.1029/2007PA001461.

Timmermann, A., S.-I. An, U. Krebs, and H. Goosse (2005), ENSO suppression due to weakening of the North Atlantic thermohaline circulation, *J. Clim.*, *18*, 3122–3139, doi:10.1175/JCLI3495.1.

Timmermann, A., et al. (2007), The influence of a weakening of the Atlantic meridional overturning circulation on ENSO, *J. Clim.*, *20*, 4899–4919, doi:10.1175/JCLI4283.1.

Tudhope, A. W., C. P. Chilcott, M. T. McCulloch, E. R. Cook, J. Chappell, R. M. Ellam, D. W. Lea, J. M. Lough, and G. B. Shimmield (2001), Variability in the El Niño-Southern Oscillation through a glacial-interglacial cycle, *Science*, *291*, 1511–1517, doi:10.1126/science.1057969.

Turney, C. S. M., A. P. Kershaw, S. C. Clemens, N. Branch, P. T. Moss, and L. K. Fifield (2004), Millennial and orbital variations of El Niño/Southern Oscillation and high-latitude climate in the last glacial period, *Nature*, *428*, 306–310.

Waelbroeck, C., L. Labeyrie, E. Michel, J. C. Duplessy, J. F. McManus, K. Lambeck, E. Balbon, and M. Labracherie (2002), Sea-level and deep water temperature changes derived from benthic foraminifera isotopic records, *Quat. Sci. Rev.*, *21*, 295–305.

Wang, C. (2001), A unified oscillator model for the El Niño–Southern Oscillation, *J. Clim.*, *14*, 98–115, doi:10.1175/1520-0442(2001)014<0098:AUOMFT>2.0.CO;2.

Wang, X., A. S. Auler, R. L. Edwards, H. Cheng, E. Ito, Y. Wang, X. Kong, and M. Solheid (2007), Millennial-scale precipitation changes in southern Brazil over the past 90000 years, *Geophys. Res. Lett.*, *34*, L23701, doi:10.1029/2007GL031149.

Yuan, D., et al. (2004), Timing, duration and transitions of the last interglacial Asian monsoon, *Science*, *304*, 575–578, doi:10.1126/science.1091220.

Zebiak, S. E., and M. A. Cane (1987), A model El Niño–Southern Oscillation, *Mon. Weather Rev.*, *115*, 2262–2278.

Zheng, W., P. Braconnot, E. Guilyardi, U. Merkel, and Y. Yu (2008), ENSO at 6 ka and 21 ka from ocean-atmosphere coupled model simulations, *Clim. Dyn.*, *30*, 745–762, doi:10.1007/s00382-007-0320-3.

E. Bard, O. Cartapanis, and L. Vidal, CEREGE, Aix-Marseille Université, Collège de France, IRD, CNRS, Europôle Méditerranéen de L'Arbois, BP 80, F-13545 Aix-en-Provence, France.

G. Leduc, Institut für Geowissenschaften, Christian Albrecht Universität, D-24118 Kiel, Germany. (gl@gpi.uni-kiel.de)